Topological states and competing magnetic fluctuations in iron germanides

Huican Mao,[*] Guangwei Wang,[*] Xiaobo Ma, Rui Liu, Pengyu Zheng, and Zhiping Yin[†]

Department of Physics and Center for Advanced Quantum Studies, Beijing Normal University, Beijing 100875, China

The correlated multiorbital multiband electronic structures of iron-based superconductors harbor an abundance of exotic electronic states, such as spin density waves, superconductivity, topological surface states, and Majorana zero modes. In this paper, we carry out density functional theory combined with dynamical mean-field theory calculations of the electronic structures, spin dynamics, and topological properties in YFe_2Ge_2 and MgFeGe and compare them with $BaFe_2As_2$ and LiFeAs. We find a coexistence of ferromagnetic and antiferromagnetic spin fluctuations in YFe_2Ge_2 and MgFeGe, which are attributed to the weakly dispersive bands just below the Fermi level. Moreover, we demonstrate that MgFeGe is in a strong topological phase and has two sets of Dirac-cone-like topological surface states on the (001) surface. The coexistence of superconductivity and nontrivial band topology in these two compounds demonstrates that it is interesting to explore topological superconductivity and Majorana zero modes in iron germanides.

I. INTRODUCTION

In recent years, the search for topological superconductivity and Majorana fermions in the solids has been at the forefront of condensed matter physics. It has been proposed that there are mainly three ways to achieve topological superconductivity: (1) intrinsic topological superconductors [1,2]; (2) a topological insulator in proximity to a conventional superconductor [3,4]; and (3) connate topological superconductors (superconductors with topological surface states) such as iron-based superconductors [5–8]. Currently, angle-resolved photoelectron spectroscopy and scanning tunneling spectroscopy experiments have confirmed the existence of surface topological superconductivity and Majorana bound states in some iron pnictides and chalcogenides, including $FeSe_{0.45}Te_{0.55}$ [9–11], $(Li_{0.84}Fe_{0.16})OHFeSe$ [12], $CaKFe_4As_4$ [13], and Li(Fe,Co)As [8,14]. However, topological surface states or Majorana zero modes in iron germanides have yet to be reported experimentally or theoretically. It is interesting to explore the existence of topological surface states in FeGe-based materials.

Since the discovery of superconductivity in $LaFeAsO_{1−x}F_x$ [15], much progress has been made in iron-based superconductors, however, the mechanism of superconductivity remains elusive. Spin fluctuations are generally considered to be involved in the superconducting pairing process. In iron pnictides and chalcogenides, predominating antiferromagnetic (AFM) spin fluctuations were widely reported, whereas much less attention was focused on ferromagnetic (FM) spin fluctuations [16]. In 2019, Wo *et al.* observed the unique coexistence of anisotropic stripe-type AFM and isotropic FM spin fluctuations in YFe_2Ge_2 by inelastic neutron scattering experiments [17]. Due to less research on FM spin fluctuations

in iron-based materials, the origin of FM spin fluctuations and the mechanism of coexisting AFM and FM spin fluctuations are still unclear in iron germanides. The relationship between superconductivity and AFM and FM spin fluctuations is also an open question in iron-based superconductors.

YFe_2Ge_2 [18], isostructural to $BaFe_2As_2$ [19], demonstrates a lower superconducting temperature of $T_c \sim 1.8$ K [20–23], and has no magnetic phase transition down to the lowest measured temperature [24]. Therefore, YFe_2Ge_2, in view of the great similarity to $BaFe_2As_2$ in the crystal structure but with a huge difference in magnetism and superconductivity, will offer us a great opportunity to study the origin of FM spin fluctuations and the coexisting mechanism of two types of spin fluctuations in iron germanides, and further explore the connection between spin fluctuations and superconductivity in iron-based materials. It is also interesting to study nonmagnetic and nonsuperconducting MgFeGe [25,26] (isostructural to the superconductor LiFeAs [27]) and compare it with YFe_2Ge_2.

II. RESULTS

In this paper, the electronic structures, spin dynamics, and topological properties of YFe_2Ge_2 and MgFeGe in the paramagnetic state are calculated based on the density functional theory plus dynamical mean-field theory (DFT+DMFT) method [28,29]. The computational details are documented in Ref. [30] and the Supplemental Material [31] (see also Refs. [32–42] therein). We find that MgFeGe is in a strong topological phase and has multiple Dirac-cone-like topological surface states on the (001) surface. Furthermore, the calculated dynamic spin structure factor demonstrates strong FM and AFM spin fluctuations in these two iron germanides. We attribute these coexisting FM and AFM spin fluctuations to the weakly dispersive bands just below the Fermi level, which indicates that they are in close proximity to a Lifshitz transition.

---

[*]These authors contributed equally to this work.
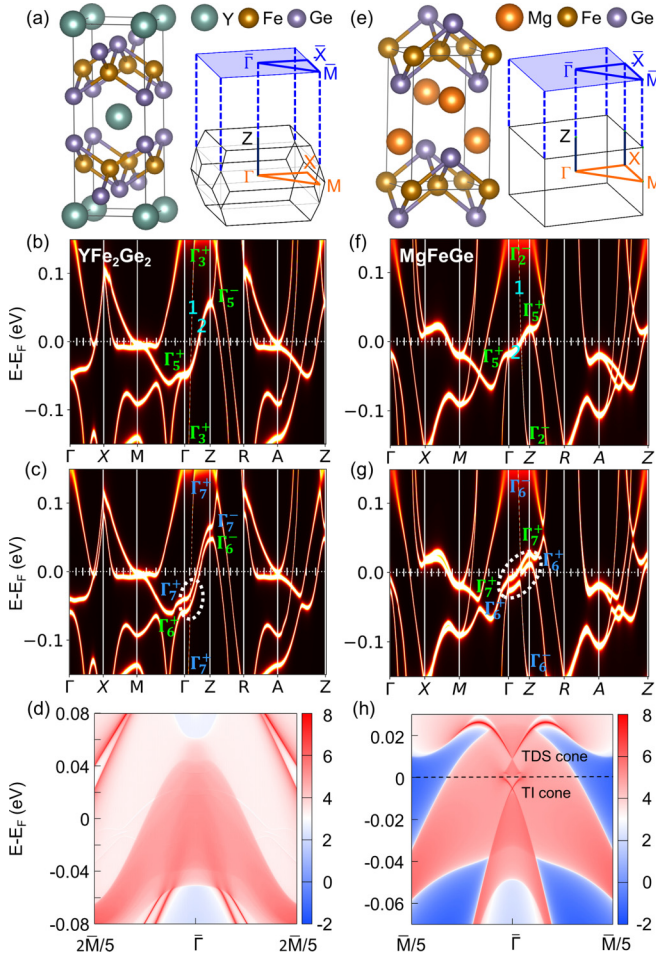[†]yinzhiping@bnu.edu.cn

FIG. 1. The crystal structures, Brillouin zones, DFT+DMFT electronic band structures, and (topological) surface states of YFe_2Ge_2 (left column) and MgFeGe (right column). (a) and (e) The crystal structure (left), and the three-dimensional and projected (001) surface Brillouin zone (right). The DFT+DMFT electronic band structures (b), (f) without and (c), (g) with spin-orbital coupling. (d) and (h) The DFT+DMFT calculated (topological) surface states on the (001) surface. No Dirac-cone-like surface state exists in (d), whereas topological Dirac semimetal cone and topological insulator cone surface states emerge in (h). All the high-symmetry points are defined in the folded Brillouin zone of the two-Fe unit cell.

A. Topological properties

We first introduce the electronic band structures and topological properties of YFe_2Ge_2 and MgFeGe, as shown in Fig. 1. Along the Γ-Z high-symmetry line, two degenerate electronic bands labeled as "2" in Figs. 1(b) and 1(f) are mostly of Fe $3d_{xz}$ and $3d_{yz}$ orbital characters for the two iron germanides, whereas the strongly dispersive electronic band labeled as "1" is dominated mainly by the Ge $4p_z$ orbital (Y $4d_{x^2-y^2}$ orbital) in MgFeGe (YFe_2Ge_2). Without a spin-orbital coupling (SOC) interaction, the two degenerate electronic bands are in Γ_5^+ states at the Γ point, and the strongly dispersive electronic band is in the Γ_2^- (Γ_3^+) state for MgFeGe (YFe_2Ge_2). When introducing the SOC interaction, the doubly degenerate Γ_5^+ states split into the Γ_6^+ state and Γ_7^+

state, and the Γ_2^- (Γ_3^+) state transforms into the Γ_6^- (Γ_7^+) state. For MgFeGe, under C_{4v} symmetry, two Ge $4p_z$ and Fe $3d_{xz/yz}$ dominated Λ_6 bands hybridize with each other and further open a gap $\sim$14 meV around the crossing point [marked by the dotted white ellipse in Fig. 1(g)], which is about 13 meV smaller than that of DFT calculations [Fig. S1(d)] due to a strong renormalization of the Fe $3d_{xz/yz}$ bands from the electronic correlation effect. Once a continuous direct SOC gap opens, we can define the Fermi curve ("curved chemical potential") through this SOC gap as shown in Fig. S1(d), and further identify the Z_2 topological invariants for all the bands below the Fermi curve [43,44]. For three-dimensional insulators, their topological properties can be characterized by four Z_2 topological invariants ($v_0; v_1v_2v_3$), where systems with $v_0 = 1$ are strong topological insulators, whereas systems with $v_0 = 0$ and $v_1^2 + v_2^2 + v_3^2 \neq 0$ are weak topological insulators [45–50]. In MgFeGe, the calculated Z_2 invariants ($v_0; v_1v_2v_3$) below the Fermi curve in Fig. S1(d) are (1; 000), which indicates it is in a strong topological phase. Notice that SOC is crucial for inducing the strong topological phase and the resulting topological surface states on the (001) surface discussed below.

In addition, the crossing between Ge $4p_z$ and Fe $3d_{xz/yz}$ dominated Λ_6 and Λ_7 bands is protected by the crystal C_{4v} symmetry, and forms a three-dimensional Dirac cone. We calculate the surface states on the (001) surface as shown in Fig. 1(h). There are two sets of topological Dirac-cone-like surface states centered at the $\bar{\Gamma}$ point: A topological insulator (TI) cone located 5 meV below the Fermi level and a topological Dirac semimetal (TDS) cone 9 meV above the Fermi level. Similar TI cone surface states had been experimentally observed in $FeSe_{0.45}Te_{0.55}$ [9], $(Li_{0.84}Fe_{0.16})OHFeSe$ [12], $CaKFe_4As_4$ [13], and Li(Fe,Co)As [8], while similar TDS cone surface states were observed in Li(Fe,Co)As [8]. If MgFeGe becomes superconducting, the topological Dirac cone surface states could harbor Majorana zero modes.

On the other hand, for YFe_2Ge_2, the strongly dispersive band 1 is mainly contributed by the Y $4d_{x^2-y^2}$ orbital with even parity (Γ_7^+) at the Γ point [Fig. 1(c)]. Here, the two Y $4d_{x^2-y^2}$ and Fe $3d_{xz/yz}$ dominated Λ_7 bands intersect with each other and further open a very tiny direct SOC gap of less than $\sim$2 meV around the crossing point [marked by the dotted white ellipse in Fig. 1(c)]. The calculated Z_2 invariants ($v_0; v_1v_2v_3$) below the Fermi curve in Fig. S1(b) are (0; 111), which indicates YFe_2Ge_2 is in a weak topological phase. In weak topological insulators, for given topological invariants ($v_0; v_1v_2v_3$) with $v_0 = 0$ and a plane with Miller indices $h(h_1, h_2, h_3)$, if h satisfies the relation ($h_i - v_i$) mod $2 = 0$ for all $i = 1, 2, 3$, the plane is topologically trivial, otherwise it is topologically nontrivial [46,51]. In YFe_2Ge_2, for the (001) surface labeled with Miller indices of a conventional unit cell, it is the ($11\bar{1}$) surface labeled with Miller indices of a primitive unit cell as shown in Figs. S2(c) and S2(d). According to the above criterion, the (001) surface of YFe_2Ge_2 is topologically trivial, hence there is no topologically protected surface state on it (see more details in Sec. D of the Supplemental Material [31]). Indeed, we do not find any topological surface states in the calculated surface states as shown in Fig. 1(d).
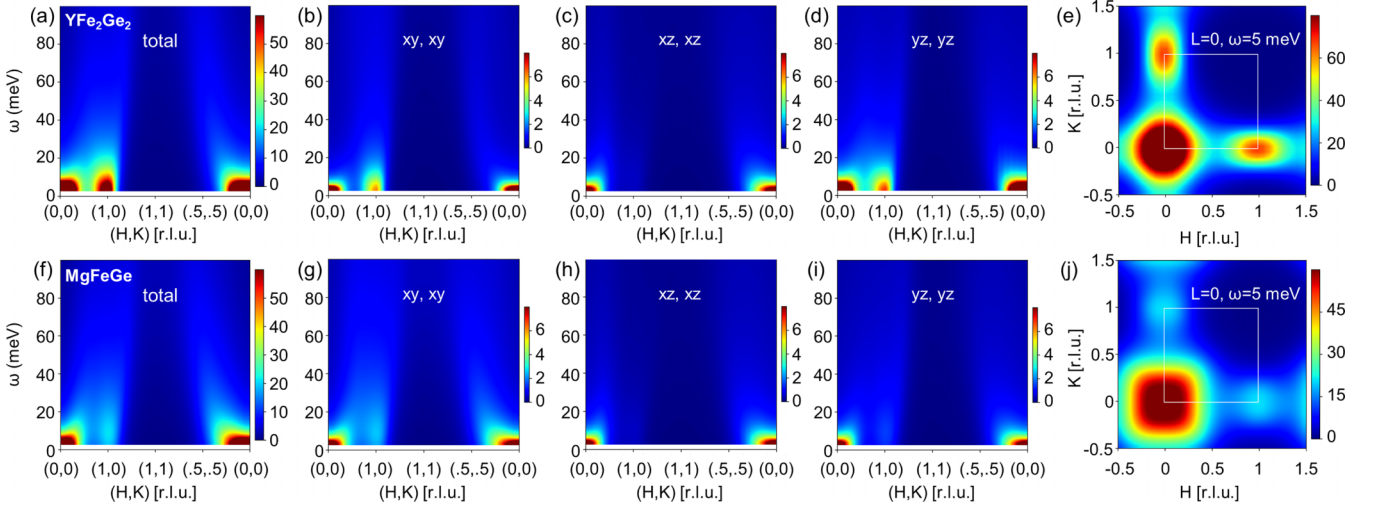
FIG. 2. The DFT+DMFT calculated dynamic spin structure factor $S(q, \omega)$ in YFe$_2$Ge$_2$ (top row) and MgFeGe (bottom row). (a) and (f) show the total $S(q, \omega)$, (b) and (g) the diagonal component $S_{xy,xy}(q, \omega)$ from the d_{xy} orbital, (c) and (h) the diagonal component $S_{xz,xz}(q, \omega)$ from the d_{xz} orbital, (d) and (i) the diagonal component $S_{yz,yz}(q, \omega)$ from the d_{yz} orbital along the high-symmetry path, and (e) and (j) the two-dimensional plots in the $L = 0$ plane with constant energy $\omega = 5$ meV. The wave vector is defined in the unfolded Brillouin zone of one-Fe unit cell.

B. Spin dynamics

Now we turn to spin fluctuations in YFe$_2$Ge$_2$ and MgFeGe. Figure 2 shows their dynamic spin structure factor $S(q, \omega)$. At low energy, there are strong intensities centered at both $q = (0, 0)$ and $q = (1, 0)$ in both YFe$_2$Ge$_2$ [Figs. 2(a) and 2(e)] and MgFeGe [Figs. 2(f) and 2(j)], which correspond to the FM and stripe AFM spin fluctuations. This is very different from most iron pnictides where the predominating AFM spin fluctuations appear at the ordering wave vector $q = (1, 0)$ of the low-temperature AFM state [16]. We note that the intensity of FM spin fluctuations is comparable to the intensity of AFM spin fluctuations in YFe$_2$Ge$_2$, in good agreement with the inelastic neutron experiments [17]. In contrast, the FM spin fluctuations are much stronger than the AFM spin fluctuations in MgFeGe.

More insight into the nature of these two types of spin fluctuations can be obtained by decomposing the dynamical spin structure factor $S(q, \omega) = \sum_{\alpha,\beta} S_{\alpha,\beta}(q, \omega)$ into different orbital contributions, where α and β are orbital indices. We find that the orbital-resolved low-energy spin excitation spectra are primarily contributed by Fe $3d$ t_{2g} orbitals. In the $L = 0$ plane with $\omega = 5$ meV, the strong FM spin fluctuations around the Brillouin zone (BZ) center $(0, 0)$ are isotropic, whereas the stripe AFM spin fluctuations near the BZ corner $(1, 0)$ show a longitudinal elongated elliptic shape, which is different from the transverse elongated elliptic shape in BaFe$_2$As$_2$.

C. Band structures and density of states

To reveal the origin of FM spin fluctuations in YFe$_2$Ge$_2$ and MgFeGe, we show their orbital- and momentum-resolved spectra $A(k, \omega)$ and density of states (DOS) and compare them with BaFe$_2$As$_2$ and LiFeAs as shown in Fig. 3. We find the bandwidth of band "3" between the M' (X) and M (M) points is 0.001 eV (0.045 eV) in YFe$_2$Ge$_2$ (MgFeGe),
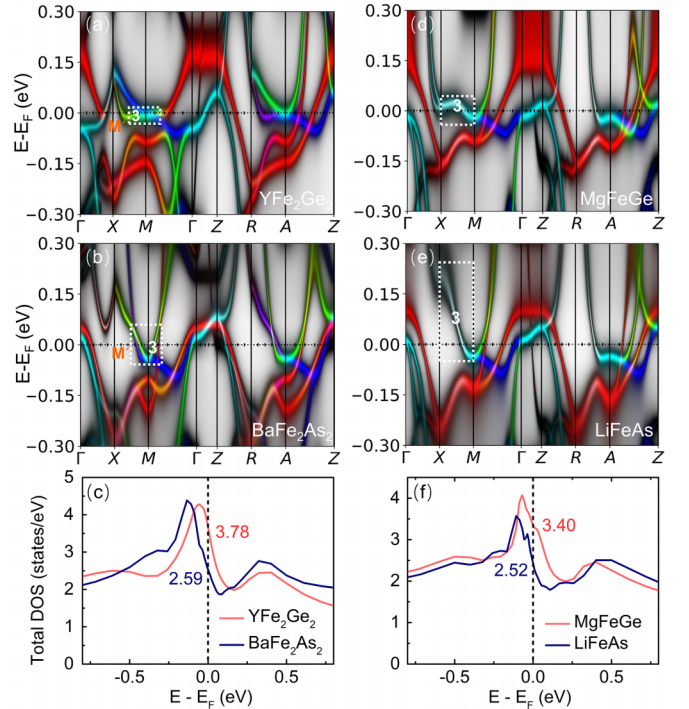

FIG. 3. The DFT + DMFT orbital- and momentum-resolved spectra $A(k, \omega)$ and density of states for YFe$_2$Ge$_2$, MgFeGe, BaFe$_2$As$_2$, and LiFeAs. (a), (b) and (d), (e) The orbital- and momentum-resolved spectra $A(k, \omega)$. (c) and (f) The total density of states. The red, green, and blue colors in $A(k, \omega)$ represent xy, xz, and yz orbitals, respectively. Band "3" around the M point is weakly dispersive, leading to a large density of states near the Fermi level in these two iron germanides. Its bandwidth is defined as the energy difference between M' (X) and M (M) points for YFe$_2$Ge$_2$ and BaFe$_2$As$_2$ (MgFeGe and LiFeAs). The M' point is defined as the midpoint between the X and M points.

which is smaller than the bandwidth of 0.099 eV (0.25 eV) in $BaFe_2As_2$ (LiFeAs). These much weakly dispersive bands in the two iron germanides will put them in close proximity to a Lifshitz transition. As a result, YFe_2Ge_2 (MgFeGe) has a 46% (35%) larger DOS than $BaFe_2As_2$ (LiFeAs) at the Fermi level as shown in Figs. 3(c) and 3(f), which suggests the iron germanides are much closer to a FM instability according to the Stoner criterion. Therefore, we attribute the strong FM spin fluctuations in YFe_2Ge_2 and MgFeGe to these weakly dispersive bands around the first BZ boundary. Furthermore, in YFe_2Ge_2, these weakly dispersive bands contributing to a large density of states near the Fermi level are consistent with several flat Fe bands around the Fermi level observed by angle-resolved photoemission spectroscopy [52] and a high Sommerfeld coefficient indicative of a large density of states near the Fermi level by heat capacity measurements [20–23]. On the other hand, the calculated band structure and density of states of MgFeGe demonstrate its metallic conduction behavior, which is in accord with transport experiments [25,26].

In order to figure out the origin of these weakly dispersive bands, we carry out a detailed comparison of the DFT hopping parameters in YFe_2Ge_2, MgFeGe, $BaFe_2As_2$, and LiFeAs, and connect them with their crystal structures and chemical properties [31]. We find that, compared to $BaFe_2As_2$, the shorter bond length of Ge-Ge (2.524 Å vs 3.788 Å) between two adjacent FeGe layers, the weaker electronegativity of the Ge element, and the higher valence state of the Fe atom ($+2.5$ vs $+2$) lead to the weakly dispersive band in YFe_2Ge_2. Meanwhile, the weakly dispersive band in MgFeGe is mainly due to the weaker electronegativity of the Ge element by comparing it with LiFeAs (see more details in Sec. E of the Supplemental Material [31]). Furthermore, electronic correlations further renormalize the Fe $3d_{xz/yz}$ band in YFe_2Ge_2 and MgFeGe, which ultimately leads to the weak dispersion of band 3 around the M point in the DFT+DMFT calculations (see more details in Sec. F of the Supplemental Material [31]).

D. Fermi surfaces

Next, we continue to analyze the origin of AFM spin fluctuations in YFe_2Ge_2 and MgFeGe using the Fermi-surface (FS) nesting picture. As shown in Fig. 4, the FSs of MgFeGe exhibit two-dimensional cylindrical features, which are very similar to those of iron pnictides [36]. The nested hole-electron FSs with dominating Fe t_{2g} orbital characters between the Fermi surfaces around the BZ center and BZ corner result in the AFM spin fluctuations in MgFeGe [Figs. 4(e) and 4(f)]. In contrast, the calculated FSs of YFe_2Ge_2 show a strong k_z dependence. In YFe_2Ge_2, there are two strongly k_z-dependent FSs marked with "4" and "5" in Fig. 4(a), which are responsible for the very large Fermi pockets of 4 and 5 in Figs. 4(b) and 4(c). These very large Fermi pockets are derived primarily from the weakly dispersive bands 3 in Fig. 3. In the Z plane, there are two circular Fermi pockets around the Z point [Fig. 4(c)], facilitating the nesting between the Fermi surfaces around the Z and A points with Fe $3d_{xz/yz}$ and $3d_{xy}$ orbital characters, whereas similar FS nesting does not happen in the Γ plane as shown in Fig. 4(b).
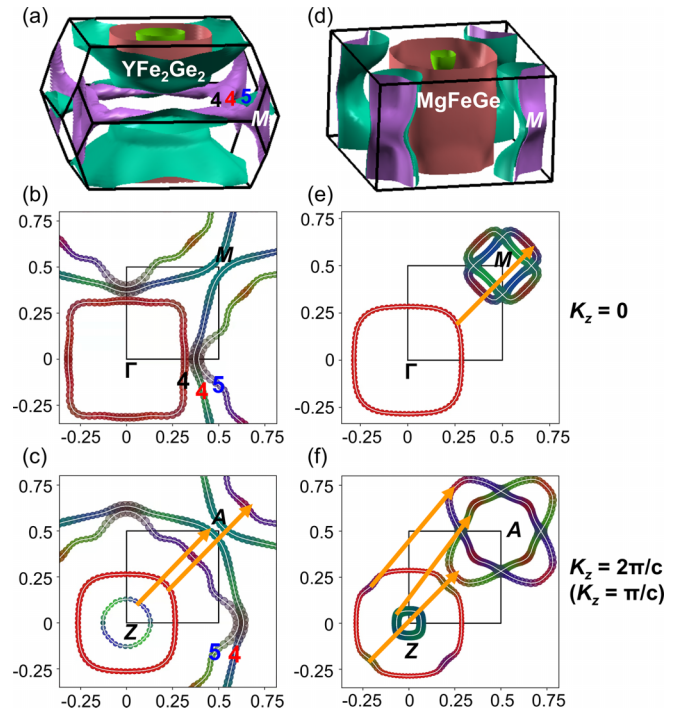

FIG. 4. The DFT+DMFT calculated three-dimensional Fermi surfaces and two-dimensional FS cuts in the Γ plane and Z plane for YFe_2Ge_2 (left column) and MgFeGe (right column). (a) and (d) Three-dimensional FSs in the paramagnetic tetragonal Brillouin zone. (b) and (e) Two-dimensional FS cuts in the Γ plane ($k_z = 0$), (c) and (f) two-dimensional FS cuts in the Z plane for YFe_2Ge_2 ($k_z = 2\pi/c$) and MgFeGe ($k_z = \pi/c$) in the folded Brillouin zone of a two-Fe unit cell. These arrows represent scattering wave vectors correlated with antiferromagnetic fluctuations. The red, green, and blue colors in two-dimensional FS cuts represent xy, xz, and yz orbitals, respectively.

III. DISCUSSIONS

In unconventional superconductors, FM spin fluctuations usually lead to spin triplet superconductivity, whereas AFM spin fluctuations tend to result in spin singlet superconductivity. The coexistence of FM and AFM spin fluctuations in YFe_2Ge_2 and MgFeGe indicates there are two competing superconducting ordering tendencies. In YFe_2Ge_2, the low superconducting temperature ($T_c \sim 1.8$ K) and the absence of long-range magnetic order down to 2 K [20–24] is likely due to the comparable intensity of FM and AFM spin fluctuations at low energies, which is in accord with inelastic neutron experiments [17]. Likewise, the competition of FM and AFM spin fluctuations at low energies in MgFeGe is detrimental to superconducting order and long-range magnetic order, which may explain the fact that no superconductivity and magnetic order were observed by transport and magnetization measurements down to 2 K [25,26]. On the other hand, the FM fluctuations are much stronger than the AFM fluctuations in MgFeGe. If we can further enhance the FM fluctuations and suppress the AFM fluctuations by means of doping and/or applying pressure, spin triplet superconductivity might be achieved in MgFeGe-derived materials.

IV. CONCLUSIONS

In conclusion, we find that the coexisting FM and AFM fluctuations in YFe$_2$Ge$_2$ and MgFeGe are mainly from the weakly dispersive bands around the BZ corner, which make them in close proximity to a Lifshitz transition. The strong FM fluctuations in MgFeGe could induce p-wave superconductivity in MgFeGe-derived materials. More importantly, our DFT+DMFT calculations indicate that MgFeGe is in a strong topological phase and has two sets of topological surface states. Therefore, iron germanides offer a potential platform for realizing topological superconductivity and Majorana zero modes.

[1] A. Y. Kitaev, Phys.-Usp. **44**, 131 (2001).

[2] L. Fu and E. Berg, Phys. Rev. Lett. **105**, 097001 (2010).

[3] L. Fu and C. L. Kane, Phys. Rev. Lett. **100**, 096407 (2008).

[4] V. Mourik, K. Zuo, S. M. Frolov, S. R. Plissard, E. P. A. M. Bakkers, and L. P. Kouwenhoven, Science **336**, 1003 (2012).

[5] G. Xu, B. Lian, P. Tang, X.-L. Qi, and S.-C. Zhang, Phys. Rev. Lett. **117**, 047001 (2016).

[6] X. Shi, Z.-Q. Han, P. Richard, X.-X. Wu, X.-L. Peng, T. Qian, S.-C. Wang, J.-P. Hu, Y.-J. Sun, and H. Ding, Sci. Bull. **62**, 503 (2017).

[7] N. Hao and J. Hu, Natl. Sci. Rev. **6**, 213 (2018).

[8] P. Zhang, Z. Wang, X. Wu, K. Yaji, Y. Ishida, Y. Kohama, G. Dai, Y. Sun, C. Bareille, K. Kuroda, T. Kondo, K. Okazaki, K. Kindo, X. Wang, C. Jin, J. Hu, R. Thomale, K. Sumida, S. Wu, K. Miyamoto *et al.*, Nat. Phys. **15**, 41 (2019).

[9] P. Zhang, K. Yaji, T. Hashimoto, Y. Ota, T. Kondo, K. Okazaki, Z. Wang, J. Wen, G. Gu, H. Ding, and S. Shin, Science **360**, 182 (2018).

[10] D. Wang, L. Kong, P. Fan, H. Chen, S. Zhu, W. Liu, L. Cao, Y. Sun, S. Du, J. Schneeloch, R. Zhong, G. Gu, L. Fu, H. Ding, and H.-J. Gao, Science **362**, 333 (2018).

[11] S. Zhu, L. Kong, L. Cao, H. Chen, M. Papaj, S. Du, Y. Xing, W. Liu, D. Wang, C. Shen, F. Yang, J. Schneeloch, R. Zhong, G. Gu, L. Fu, Y.-Y. Zhang, H. Ding, and H.-J. Gao, Science **367**, 189 (2020).

[12] Q. Liu, C. Chen, T. Zhang, R. Peng, Y.-J. Yan, C.-H.-P. Wen, X. Lou, Y.-L. Huang, J.-P. Tian, X.-L. Dong, G.-W. Wang, W.-C. Bao, Q.-H. Wang, Z.-P. Yin, Z.-X. Zhao, and D.-L. Feng, Phys. Rev. X **8**, 041056 (2018).

[13] W. Liu, L. Cao, S. Zhu, L. Kong, G. Wang, M. Papaj, P. Zhang, Y.-B. Liu, H. Chen, G. Li, F. Yang, T. Kondo, S. Du, G.-H. Cao, S. Shin, L. Fu, Z. Yin, H.-J. Gao, and H. Ding, Nat. Commun. **11**, 5688 (2020).

[14] L. Kong, L. Cao, Z. Shiyu, M. Papaj, G. Dai, G. Li, P. Fan, W. Liu, F. Yang, X. Wang, S. Du, C. Jin, L. Fu, H.-J. Gao, and H. Ding, Nat. Commun. **12**, 4146 (2021).

[15] Y. Kamihara, T. Watanabe, M. Hirano, and H. Hosono, J. Am. Chem. Soc. **130**, 3296 (2008).

[16] P. Dai, Rev. Mod. Phys. **87**, 855 (2015).

[17] H. Wo, Q. Wang, Y. Shen, X. Zhang, Y. Hao, Y. Feng, S. Shen, Z. He, B. Pan, W. Wang, K. Nakajima, S. Ohira-Kawamura, P. Steffens, M. Boehm, K. Schmalzl, T. R. Forrest, M. Matsuda, Y. Zhao, J. W. Lynn, Z. Yin, and J. Zhao, Phys. Rev. Lett. **122**, 217003 (2019).

[18] G. Venturini and B. Malaman, J. Alloy. Compd. **235**, 201 (1996).

[19] M. Rotter, M. Tegel, D. Johrendt, I. Schellenberg, W. Hermes, and R. Pöttgen, Phys. Rev. B **78**, 020503(R) (2008).

[20] Y. Zou, Z. Feng, P. Logg, J. Chen, G. Lampronti, and F. Grosche, Phys. Status Solidi RRL **8**, 928 (2014).

[21] J. Chen, K. Semeniuk, Z. Feng, P. Reiss, P. Brown, Y. Zou, P. W. Logg, G. I. Lampronti, and F. M. Grosche, Phys. Rev. Lett. **116**, 127001 (2016).

[22] J. Chen, M. B. Gamża, K. Semeniuk, and F. M. Grosche, Phys. Rev. B **99**, 020501(R) (2019).

[23] J. Baglo, J. Chen, K. Murphy, R. Leenen, A. McCollam, M. L. Sutherland, and F. M. Grosche, Phys. Rev. Lett. **129**, 046402 (2022).

[24] M. Avila, S. Bud'ko, and P. Canfield, J. Magn. Magn. Mater. **270**, 51 (2004).

[25] X. Liu, S. Matsuishi, S. Fujitsu, and H. Hosono, Phys. Rev. B **85**, 104403 (2012).

[26] R. Welter, B. Malaman, and G. Venturini, Solid State Commun. **108**, 933 (1998).

[27] J. H. Tapp, Z. Tang, B. Lv, K. Sasmal, B. Lorenz, P. C. W. Chu, and A. M. Guloy, Phys. Rev. B **78**, 060505(R) (2008).

[28] G. Kotliar, S. Y. Savrasov, K. Haule, V. S. Oudovenko, O. Parcollet, and C. A. Marianetti, Rev. Mod. Phys. **78**, 865 (2006).

[29] K. Haule, C.-H. Yee, and K. Kim, Phys. Rev. B **81**, 195107 (2010).

[30] X. Ma, G. Wang, R. Liu, T. Yu, Y. Peng, P. Zheng, and Z. Yin, Phys. Rev. B **106**, 115114 (2022).

[31] See Supplemental Material at http://link.aps.org/supplemental/10.1103/PhysRevB.107.115116 for computational methods, topological phase and hopping parameters.

[32] P. Blaha, K. Schwarz, G. K. Madsen, D. Kvasnicka, and J. Luitz, *WIEN2K, An Augmented Plane Wave+Local Orbitals Program for Calculating Crystal Properties* (Karlheinz Schwarz, Vienna University of Technology, Austria, 2001).

[33] Z. P. Yin, K. Haule, and G. Kotliar, Nat. Phys. **10**, 845 (2014).

[34] K. Haule, Phys. Rev. B **75**, 155113 (2007).

[35] P. Werner, A. Comanac, L. de' Medici, M. Troyer, and A. J. Millis, Phys. Rev. Lett. **97**, 076405 (2006).

[36] Z. Yin, K. Haule, and G. Kotliar, Nat. Mater. **10**, 932 (2011).

[37] Z. Yin, K. Haule, and G. Kotliar, Nat. Phys. **7**, 294 (2011).

[38] Y. Li, Z. Yin, X. Wang, D. W. Tam, D. L. Abernathy, A. Podlesnyak, C. Zhang, M. Wang, L. Xing, C. Jin, K. Haule, G. Kotliar, T. A. Maier, and P. Dai, Phys. Rev. Lett. **116**, 247001 (2016).

[39] C. Zhang, L. W. Harriger, Z. Yin, W. Lv, M. Wang, G. Tan, Y. Song, D. L. Abernathy, W. Tian, T. Egami, K. Haule, G. Kotliar, and P. Dai, Phys. Rev. Lett. **112**, 217202 (2014).

[40] N. Marzari, A. A. Mostofi, J. R. Yates, I. Souza, and D. Vanderbilt, Rev. Mod. Phys. **84**, 1419 (2012).

[41] A. A. Mostofi, J. R. Yates, G. Pizzi, Y.-S. Lee, I. Souza, D. Vanderbilt, and N. Marzari, Comput. Phys. Commun. **185**, 2309 (2014).

[42] Q. Wu, S. Zhang, H.-F. Song, M. Troyer, and A. A. Soluyanov, Comput. Phys. Commun. **224**, 405 (2018).

[43] Z. Wang, P. Zhang, G. Xu, L. K. Zeng, H. Miao, X. Xu, T. Qian, H. Weng, P. Richard, A. V. Fedorov, H. Ding, X. Dai, and Z. Fang, Phys. Rev. B **92**, 115119 (2015).

[44] S. Nie, L. Xing, R. Jin, W. Xie, Z. Wang, and F. B. Prinz, Phys. Rev. B **98**, 125143 (2018).

[45] J. E. Moore and L. Balents, Phys. Rev. B **75**, 121306(R) (2007).

[46] L. Fu, C. L. Kane, and E. J. Mele, Phys. Rev. Lett. **98**, 106803 (2007).

[47] L. Fu and C. L. Kane, Phys. Rev. B **76**, 045302 (2007).

[48] R. Roy, Phys. Rev. B **79**, 195322 (2009).

[49] M. Z. Hasan and C. L. Kane, Rev. Mod. Phys. **82**, 3045 (2010).

[50] X.-L. Qi and S.-C. Zhang, Rev. Mod. Phys. **83**, 1057 (2011).

[51] Z. Ringel, Y. E. Kraus, and A. Stern, Phys. Rev. B **86**, 045102 (2012).

[52] D. F. Xu, D. W. Shen, D. Zhu, J. Jiang, B. P. Xie, Q. S. Wang, B. Y. Pan, P. Dudin, T. K. Kim, M. Hoesch, J. Zhao, X. G. Wan, and D. L. Feng, Phys. Rev. B **93**, 024506 (2016).